Available online at www.sciencedirect.com
ScienceDirect
Mathematics and Computers in Simulation 81 (2011) 2326–2336
MATHEMATICS AND COMPUTERS IN SIMULATION
www.elsevier.com/locate/matcom

Original article

A mathematical model of atmospheric retention of man-made CO_2 emissions

Bert W. Rust *

National Institute of Standards and Technology, Gaithersburg, MD 20899-8910, USA

Received 20 November 2009; received in revised form 28 June 2010; accepted 8 December 2010
Available online 21 December 2010

Abstract

Rust and Thijsse have previously shown that changes in global annual average temperature anomalies $T(t_i)$ compiled by the Climatic Research Unit vary linearly with atmospheric CO_2 concentrations $c(t_i)$. The $c(t_i)$ can be related to man-made CO_2 emissions $F(t_i)$ by a linear regression model whose solution vector gives the unknown retention fractions $\gamma(t_i)$ of the $F(t_i)$ in the atmosphere. Gaps in the $c(t_i)$ record make the system underdetermined, but the constraints $0 \le \gamma(t_i) \le 1$ make estimation tractable. The $\gamma(t_i)$ are estimated by two methods: (1) assuming a finite harmonic expansion for $\gamma(t)$, and (2) using a constrained least squares algorithm to compute average values of $\gamma(t)$ on suitably chosen time subintervals. The final result is an estimate of $\gamma(t)$ with enough accuracy to establish the connection between emissions from fossil fuel use and land use changes and increases in global average annual temperature anomalies.
Published by Elsevier B.V. on behalf of IMACS.

Keywords: CO_2 emissions; Atmospheric CO_2; Global temperatures; Global warming

1. Atmospheric CO_2 and global temperatures

Throughout this paper the terms *warming* and *global warming* will be used to refer to the well documented [8] increases in global average annual temperature anomalies from 1850 to the present. Uncertainties in global climate models are often used to cast doubt on the reality of global warming, but complicated climate models are not needed to establish that reality. Rust and Thijsse [14,16] have used the measurements of global average temperatures and of atmospheric carbon dioxide concentrations to confirm that the warming is real and that it is principally caused by the increasing CO_2 concentrations.

The plot in Fig. 1 gives the record of atmospheric CO_2 concentrations obtained by combining atmospheric measurements (1958–2004) at the South Pole [9] with reconstructions (1647–1978) from Antarctic ice cores [4,11]. Although the latter display larger random variations than the former, the two records are consistent in the years where they overlap. The horizontal dashed line at $c_0 = 277.04$ ppmv is the preindustrial CO_2 concentration estimated by averaging the ice-core measurements for 1647–1764. The solid curve is a cubic regression spline fit obtained from Thijsse's *spline2* program [16] which chooses the number and locations of the knots to give an optimal separation of signal from noise. It will be used in the following as the functional representation $c(t)$ of the concentration measurements.

* Tel.: +1 301 975 3811; fax: +1 301 975 3553.
E-mail address: bert.rust@nist.gov

0378-4754/$36.00 Published by Elsevier B.V. on behalf of IMACS.
doi:10.1016/j.matcom.2010.12.019

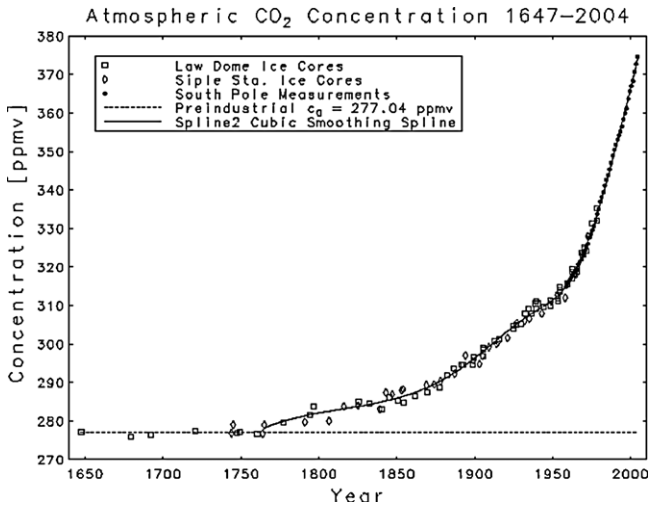

Fig. 1. Atmospheric CO_2 concentrations measured in units of parts per million by volume.

The time series data plotted in Fig. 2 are the Climatic Research Unit's record [8] of annual average global surface temperature anomalies. Rust and Thijsse assumed [14] that changes in the temperature anomaly were linearly proportional to changes in the atmospheric concentration of CO_2, i.e., that

$$\frac{\mathrm{d}T}{\mathrm{d}t} = \eta \frac{\mathrm{d}c}{\mathrm{d}t}, \tag{1}$$

where η is a constant to be determined by fitting. Choosing the time scale so that $t = 0$ at epoch 1856.0, and integrating the above equation give

$$T(t) = T_0 + \eta\,[c(t) - c_0]\,, \tag{2}$$

where $c_0 = 277.04$ is the preindustrial concentration illustrated in Fig. 1 and T_0 is the corresponding temperature anomaly (not the temperature anomaly at $t = 0$) which is also estimated by fitting. Fitting the above expression to the measured data in Fig. 2 would give a curve very similar to the dashed curve that is plotted there, but that curve was

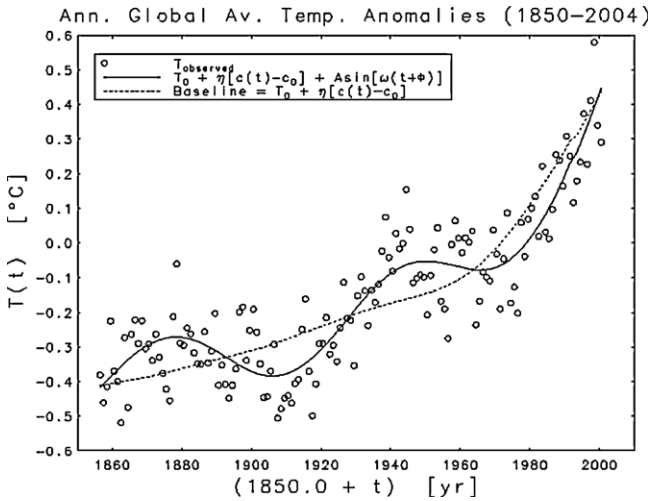

Fig. 2. Annual global average temperature anomalies. The anomaly for any given year was obtained by subtracting a reference temperature from the average temperature for that year. The reference temperature used here was the average temperature for the years 1961–1990. The solid curve is the fit of the model (3) to the data, and the dashed curve is a plot of $\hat{T}_0 + \hat{\eta}[c(t) - 277.04]$ where $\hat{T}_0$ and $\hat{\eta}$ are the parameter estimates obtained from that fit. The angular frequency ω in the legend was computed from the estimate of the period τ in (3).

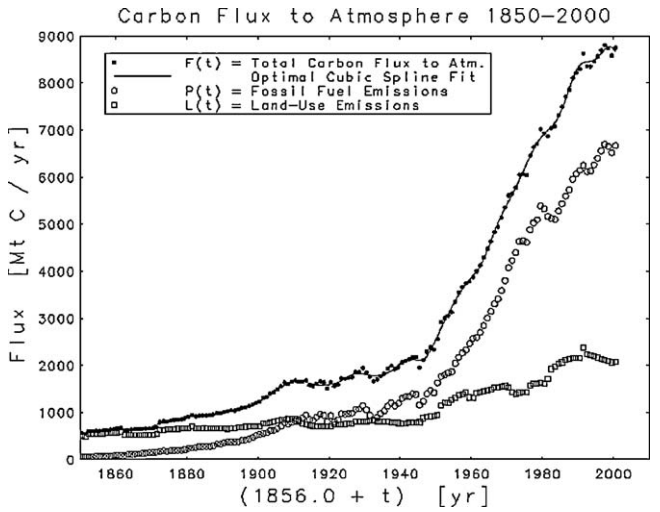

Fig. 3. Annual man-made carbon emissions to the atmosphere. The flux units are megatons of carbon per year. The spline fit in the upper plot, which was gotten from Thijsse's *spline2* [16], will be used in the following as a functional representation of $F(t)$.

actually obtained by fitting the model

$$T(t) = T_0 + \eta[c(t) - 277.04] + A \sin\left[\frac{2\pi}{\tau}(t + \phi)\right], \tag{3}$$

with free parameters T_0, η, A, τ, and ϕ. The sinusoid in this model represents the $\approx$ 70 year oscillation discovered in 1994 by Schlesinger and Ramankutty [15]. Statistical tests leave no doubt about the reality of this oscillation, but its cause is unknown.

The solid curve in Fig. 2 is the nonlinear least squares fit of the model (3) to the data. The parameter estimates and their standard uncertainties, which were obtained from the usual quadratic approximation [1] to the least squares response function in the neighborhood of the estimate vector, were

$$\begin{aligned}
&\hat{T}_0 = (-0.507 \pm .016)\,(^\circ\mathrm{C}),\\
&\hat{\eta} = (0.01039 \pm .00042)\,(^\circ\mathrm{C/ppmv}),\\
&\hat{A} = (0.099 \pm .012)\,(^\circ\mathrm{C}),\\
&\hat{\tau} = (71.5 \pm 2.2)\,(\mathrm{year}),\\
&\hat{\phi} = (-1.0 \pm 1.4)\,(\mathrm{year}),
\end{aligned} \tag{4}$$

and the sum of squared residuals and coefficient of determination were

$$\mathrm{SSR} = 1.2674 \quad \text{and} \quad R^2 = 0.8519,$$

so the model explains $\approx$85% of the variance in the data. The sinusoid accounts for $\approx$8% of that variance, and the baseline $\hat{T}_0 + \hat{\eta}[c(t) - 277.04]$ accounts for $\approx$77%. The baseline indicates that: (1) *there is a linear relationship between global warming and increasing atmospheric CO_2*, (2) the total warming since 1856 has been $\approx$0.9 °C, and (3) *that the warming is accelerating*.

2. Man-made carbon emissions to the atmosphere

Annual total man-made carbon emissions to the atmosphere, for the years 1850–2000, are shown in the upper curve in Fig. 3. The total $F(t)$ is the sum of annual fossil fuel emissions $P(t)$ [10] and emissions $L(t)$ due to changes in land use [7]. In order to compare these emissions with the atmospheric concentrations plotted in Fig. 1, it is necessary to use the unit conversion relationship 1 ppmv = 2130 Mt C [3, p. 467]. Knowing that, the people at the Carbon Dioxide Information Analysis Center were able to show [2] that in the period 1850–2000, the total man-made CO_2 emissions to the atmosphere were 44,150 Mt C and that the total increase in atmospheric CO_2 was 17,400 Mt C. Thus, on average, approximately 39 % of the emissions in any given year remains in the atmosphere. Actually, the fraction remaining in

the atmosphere is not constant over time. Since $t=0$ at epoch 1856.0, then $t=-6$ at epoch 1850.0, and for any later time t, the atmospheric concentration would be

$$c(t) = c_{1850} + \int_{-6}^{t} \gamma(\tau)F(\tau)\,\mathrm{d}\tau, \tag{5}$$

where $\gamma(\tau)$ is the unknown fraction remaining in the atmosphere. It is important to note that $\gamma(\tau)$ must satisfy the constraints

$$0 \le \gamma(\tau) \le 1, \quad \text{for all } \tau \text{ satisfying } 1850 \le 1856 + \tau \le 2000. \tag{6}$$

Since the eruption of Mt. Pinatubo on June 15, 1991 had a discernible effect on $c(t)$ for the two succeeding years, a more precise model is

$$c(t) = c_{1850} + \int_{-6}^{t} \gamma(\tau)F(\tau)\,\mathrm{d}\tau + \delta S(t), \tag{7}$$

where $S(t)$ is the declining ramp function

$$S(t) = \begin{cases} 0, & 1856 + t < 1991.54, \\ -\dfrac{1}{2}(1856 + t - 1991.54), & 1991.54 \le 1856 + t \le 1993.54, \\ -1, & 1993.54 < 1856 + t, \end{cases} \tag{8}$$

and δ is an unknown amplitude constant to be determined by fitting. The ramp function declines because aerosols injected into the atmosphere by the eruption diffused the incoming sunlight in a way which increased the photosynthetic uptake of CO_2 by the biosphere [6].

Although the unknown constants c_{1850} and δ complicate the problem, Eq. (7) is basically a first kind integral equation. Estimating the solution is difficult because that solution is exquisitely sensitive to errors in the measured function $c(t)$. There are two approaches to estimating $\gamma(\tau)$: (1) estimating the parameters in a finite parametric approximation of $\gamma(\tau)$ and (2) solving the *inverse problem* directly.

3. Finite harmonic approximations

Parametric approximations usually assume that $\gamma(\tau)$ can be approximated by a finite linear combination of (usually orthogonal) basis functions and seeks to estimate the coefficients in that combination by fitting it to the measurements $c(t_i)$. For the present problem, it is natural to define angular frequencies

$$\omega_k \equiv \frac{2\pi k}{150}, \quad k = 1, 2, \ldots, n_h, \tag{9}$$

and assume a harmonic expansion

$$\gamma(t) = A_0 + \sum_{k=1}^{n_h} [A_k\, \cos(\omega_k t) + B_k\, \sin(\omega_k t)], \quad 1850 \le t \le 2000, \tag{10}$$

with unknown parameters A_0, A_k, B_k. Substituting this expansion into (7) and discretizing the relation to the years t_i in which actual observations $c(t_i)$ are available gives

$$\begin{aligned} c(t_i) = c_{1850} + A_0 \int_{-6}^{t_i} F(\tau)\,\mathrm{d}\tau + \sum_{k=1}^{n_h} A_k \int_{-6}^{t_i} \cos(\omega_k \tau)F(\tau),\,\mathrm{d}\tau \\ + \sum_{k=1}^{n_h} B_k \int_{-6}^{t_i} \sin(\omega_k \tau)F(\tau)\,\mathrm{d}\tau + \delta S(t_i), \quad i = 1, 2, \ldots, 119, \end{aligned} \tag{11}$$

where the indicated integrals can be evaluated by using the spline fit in the top plot of Fig. 3 to represent $F(\tau)$. Clearly n_h must be chosen so that $2n_h + 3$ is less than the number of observed $c(t_i)$. Such a choice leads to a linear least squares problem which can be solved to get estimates for c_0, δ, and the A_k and B_k. Choosing n_h too large produces implausibly oscillating estimates for $\gamma(t)$ which violate the constraints $0 \le \gamma(t) \le 1$.

Table 1
F-test results for the fits in Fig. 4.

n_h	H_0	SSR	u	$F_{0.95}$	Action
0		291.906			
1	$A_1 = 0, B_1 = 0$	124.381	76.7715	3.0759	Reject H_0
2	$A_2 = 0, B_2 = 0$	107.959	8.5185	3.0773	Reject H_0
3	$A_3 = 0, B_3 = 0$	98.506	5.2780	3.0788	Reject H_0
4	$A_4 = 0, B_4 = 0$	93.366	2.9730	3.0804	Accept H_0

The appropriate value for n_h was chosen by successively fitting Eq. (11) with $n_h = 0, 1, 2, \ldots$ and, for each fit after the first, checking whether or not the two new parameters produced a statistically significant reduction in the sum of squared residuals. The results from this procedure are summarized in Table 1 where the second column gives the null hypothesis H_0 that is tested at each step of the procedure. The third column gives the sum of squared residuals SSR for the fit and the fourth column gives the statistic

$$u = \frac{(\mathrm{SSR})_H - (\mathrm{SSR})_F}{(\mathrm{SSR})_F} \cdot \frac{m-n}{k},$$

where $(\mathrm{SSR})_F$ is the SSR for the full model (on the same line in the table) and $(\mathrm{SSR})_H$ is the SSR for the hypothesis model (on the previous line in the table). The value $m = 119$ is the number of measured $[t_i, c(t_i)]$ data points, the value $n = 2n_h + 3$ is the number of free parameters in the full model, and the value $k = 2$ is the number of degrees of freedom associated with H_0. The fifth column of the table gives the 0.95 percentile of the $F(k, m-n)$ probability distribution. The F-test compares this value with the u-statistic from column 4 and rejects H_0 so long as $u > F_{0.95}$. The table clearly indicates that $n_h = 3$ is the best choice for the number of harmonics in the model.

The fits for $n_h = 0, 1, 2,$ and 3 are plotted in Fig. 4 and the corresponding estimates of the function $\gamma(t)$ are plotted in Fig. 5 using the same color coding. For the best fit ($n_h = 3$) the parameter estimates, and their standard uncertainties [5, Section 6.5] were

$$\begin{aligned}
&\hat{c}_{1850} = 285.69 \pm .40 && \hat{A}_0 = 0.4369 \pm .0094 \\
&\hat{A}_1 = 0.062 \pm .019 && \hat{B}_1 = 0.116 \pm .013 \\
&\hat{A}_2 = -0.000086 \pm .019257 && \hat{B}_2 = -0.0029 \pm .0225 \\
&\hat{A}_3 = -0.060 \pm .019 && \hat{B}_3 = 0.018 \pm .018 \\
& && \hat{\delta} = -1.59 \pm .96.
\end{aligned} \tag{12}$$

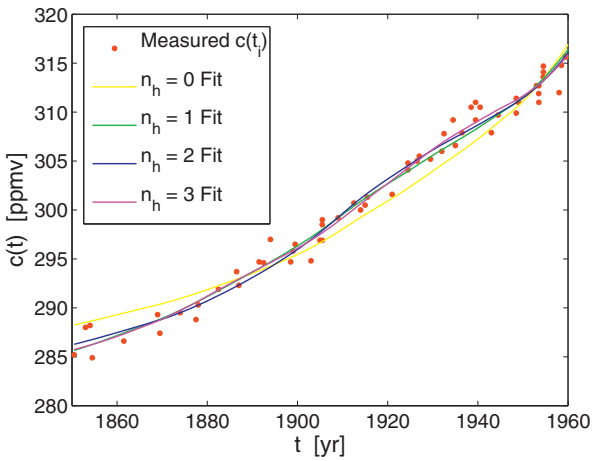

Fig. 4. Harmonic approximation fits to the atmospheric CO_2 concentrations for the period 1850–1960. After 1960 the extremely precise atmospheric measurements from the South Pole dominate the fits, causing them all to merge so closely that it is difficult to distinguish the separate curves.

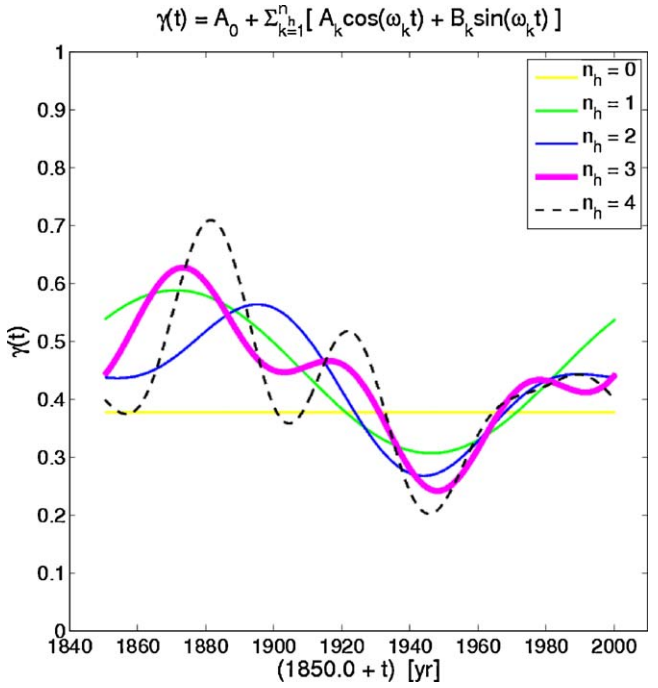

Fig. 5. Fraction of CO_2 emissions remaining in the atmosphere.

With SSR = 98.506, the coefficient of determination was $R^2 = 0.9979$ which means that the fit explains 99.79% of the variance in the data.

4. The inverse problem

Since there are 83 independent measurements of $c(t)$ in the interval $1850 \le t \le 2000$, Eq. (7) can be replaced by

$$c(t_i) = c_{1850} + \int_{1850}^{t_i} \gamma(\tau) F(\tau)\, \mathrm{d}\tau + \delta S(t_i) + \epsilon_i, \quad i = 1, 2, \ldots, 83, \tag{13}$$

where the ϵ_i are the measurement errors which are assumed to be independently normally distributed with means zero and a diagonal covariance matrix $\boldsymbol{\Sigma}^2$. In choosing the 83 measurements, we discarded the ice core reconstructions in the time interval overlapping the atmospheric measurements because the latter are much more accurate than the former. To determine $\boldsymbol{\Sigma}^2$ we assumed constant variance for each of the two subsets of data and estimated those two variances from the deviations of the data from two separately fitted optimal smoothing splines obtained from *spline2* [16]. Those fits and the calculated standard uncertainties,

$$\sigma_i = 1.0888, \quad i = 1, 2, \ldots, 40 \qquad \text{and} \qquad \sigma_i = 0.2552, \quad i = 41, 42, \ldots, 83,$$

are plotted in Fig. 6.

For the inverse problem, the integrals in (13) are approximated with quadrature sums. Choosing $\Delta\tau = 1$, replacing the continuous variable τ with a mesh

$$\tau_j = 1850.0 + (j-1)\Delta\tau, \quad j = 1, 2, \ldots, 151,$$

and using a rectangular quadrature rule gives

$$c(t_i) = c_{1850} + \sum_{j=1}^{151} \gamma(\tau_j) F(t_i, \tau_j) \Delta\tau + \delta S(t_i) + \epsilon_i, \quad i = 1, 2, \ldots, 83, \tag{14}$$

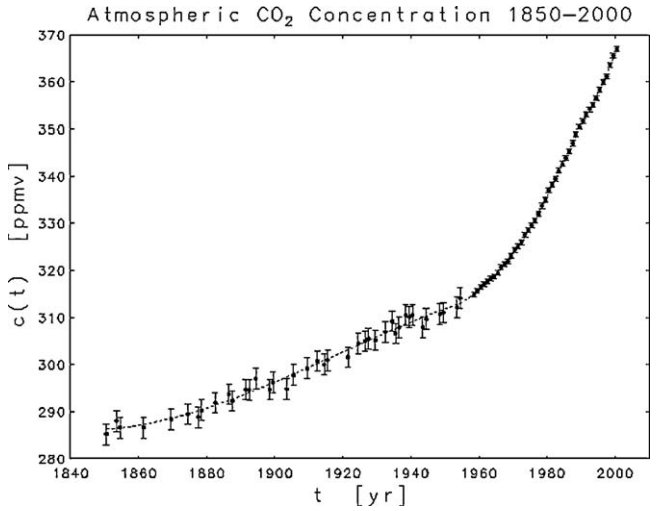

Fig. 6. Atmospheric CO_2 concentrations with their standard uncertainties. The dashed curve is a plot of the two *spline2* fits.

where

$$F(t_i, \tau_j) = \begin{cases} F(\tau_j), & \tau_j \le t_i, \\ 0, & \tau_j > t_i, \end{cases} \qquad j = 1, 2, \ldots, 151, \quad i = 1, 2, \ldots, 83. \tag{15}$$

Writing Eq. (14) in vector-matrix notation gives

$$\mathbf{c} = [\mathbf{1}, \mathbf{F}, \boldsymbol{s}] \begin{bmatrix} c_{1850} \\ \boldsymbol{\gamma} \\ \delta \end{bmatrix} + \boldsymbol{\epsilon}, \quad \boldsymbol{\epsilon} \sim N(\mathbf{0}, \boldsymbol{\Sigma}^2), \tag{16}$$

where $\boldsymbol{c}$ is an order-83 column vector of concentration measurements, $\boldsymbol{1}$ is a vector of ones, $\boldsymbol{F}$ is the 83×151 matrix defined by (15), $\boldsymbol{s}$ is a vector whose elements are defined by the ramp function (8), $\boldsymbol{\gamma}$ is an unknown, order-151 column vector whose elements define a discrete approximation to the function $\gamma(t)$, and ϵ is a vector of measurement errors. This is a highly underdetermined linear regression model, but estimation is possible because $\boldsymbol{0} \le \boldsymbol{\gamma} \le \boldsymbol{1}$, and it is easy to see from the concentration data that $280 \le c_{1850} \le 290$ and $0 \le \delta \le 3$. These box constraints can be incorporated into the model by a regularization method [13], to be described below, which biases the estimate to lie close to the center of the box.

To simplify the notation, premultiply (16) by $\boldsymbol{\Sigma}^{-1}$, and define

$$\boldsymbol{b} \equiv \boldsymbol{\Sigma}^{-1}\boldsymbol{c}, \quad \boldsymbol{A} \equiv \boldsymbol{\Sigma}^{-1}[\mathbf{1}, \mathbf{F}, \boldsymbol{s}], \quad \boldsymbol{x} \equiv \begin{bmatrix} c_{1850} \\ \boldsymbol{\gamma} \\ \delta \end{bmatrix}, \quad \boldsymbol{\eta} \equiv \boldsymbol{\Sigma}^{-1}\boldsymbol{\epsilon}, \tag{17}$$

to get

$$\boldsymbol{b} = \boldsymbol{A}\boldsymbol{x} + \boldsymbol{\eta}, \quad \boldsymbol{\eta} \sim N(\mathbf{0}, \boldsymbol{I}_{83}), \tag{18}$$

where $\boldsymbol{I}_{83}$ is the order-83 identity matrix. And defining the order-153 vectors

$$\boldsymbol{p} \equiv (280, 0, 0, \ldots, 0, 0)^T, \tag{19}$$

$$\boldsymbol{q} \equiv (290, 1, 1, \ldots, 1, 3)^T, \tag{20}$$

allows the box constraints to be written

$$\Pr\{\boldsymbol{p} \le \boldsymbol{x} \le \boldsymbol{q}\} = 1.0. \tag{21}$$

A method for incorporating this kind of *a priori* information into the estimate for $\boldsymbol{x}$ was developed many years ago by Pierce and Rust [13]. That method, which was named *FERDIT*, replaces (18) with a *regularized model*

$$\begin{pmatrix} \boldsymbol{b} \\ \lambda \boldsymbol{Q}^{-1}\boldsymbol{d} \end{pmatrix} = \begin{pmatrix} \boldsymbol{A} \\ \lambda \boldsymbol{Q}^{-1} \end{pmatrix} \boldsymbol{x}(\lambda) + \begin{pmatrix} \boldsymbol{\eta} \\ \lambda \boldsymbol{\mu} \end{pmatrix}, \quad \begin{pmatrix} \boldsymbol{\eta} \\ \lambda \boldsymbol{\mu} \end{pmatrix} \sim N\left[\begin{pmatrix} \boldsymbol{0} \\ \boldsymbol{0} \end{pmatrix}, \begin{pmatrix} \boldsymbol{I}_{83} & \boldsymbol{O} \\ \boldsymbol{O} & \boldsymbol{I}_{153} \end{pmatrix} \right], \tag{22}$$

where

$$\boldsymbol{d} \equiv (285, 0.5, 0.5, \ldots, 0.5, 1.5)^T \tag{23}$$

is the center of the box,

$$\boldsymbol{Q} \equiv \mathbf{diag}(5.0, 0.5, 0.5, \ldots, 0.5, 1.5) \tag{24}$$

has diagonal elements equal to the half widths of the sides of the box, and λ is a *regularization parameter* which must be chosen from the interval $0 \le \lambda < \infty$. Having made that choice, it is easy to see that the regularized estimate is

$$\tilde{\boldsymbol{x}}(\lambda) = [\boldsymbol{A}^T\boldsymbol{A} + \lambda^2 \boldsymbol{Q}^{-2}]^{-1}[\boldsymbol{A}^T\boldsymbol{b} + \lambda^2 \boldsymbol{Q}^{-2}\boldsymbol{d}]. \tag{25}$$

For any λ, this is a biased estimate, biased toward the center $\boldsymbol{d}$ of the bounding box, with the strength of the bias determined by the value of λ. As with most regularization methods, a wide range of λ values give similar good results, but it is possible to choose an optimal λ by a method to be described in the following.

The *FERDIT* method was originally designed to compute suboptimal, but conservative, confidence intervals for each element of $\boldsymbol{x}$. Suppose that $\boldsymbol{w}$ is a given n-vector and the goal is to compute a confidence interval for $\phi = \boldsymbol{w}^T\boldsymbol{x}$ which holds with probability α. Classical linear regression theory solves this problem by first computing a least squares estimate

$$\hat{\boldsymbol{x}} = arg\min\{(\boldsymbol{b} - \boldsymbol{A}\boldsymbol{x})^T(\boldsymbol{b} - \boldsymbol{A}\boldsymbol{x})\}, \quad r_0 \equiv \min_{\boldsymbol{x}}\{(\boldsymbol{b} - \boldsymbol{A}\boldsymbol{x})^T(\boldsymbol{b} - \boldsymbol{A}\boldsymbol{x})\}, \tag{26}$$

and then choosing the α level percentile κ from the standard normal distribution and defining

$$\hat{\phi}_{lo} = \min_{\boldsymbol{x}}\{\boldsymbol{w}^T\boldsymbol{x} | (\boldsymbol{b} - \boldsymbol{A}\boldsymbol{x})^T(\boldsymbol{b} - \boldsymbol{A}\boldsymbol{x}) \le r_0 + \kappa^2\}, \tag{27}$$

$$\hat{\phi}^{up} = \max_{\boldsymbol{x}}\{\boldsymbol{w}^T\boldsymbol{x} | (\boldsymbol{b} - \boldsymbol{A}\boldsymbol{x})^T(\boldsymbol{b} - \boldsymbol{A}\boldsymbol{x}) \le r_0 + \kappa^2\}, \tag{28}$$

to be the extreme values of $\boldsymbol{w}^T\boldsymbol{x}$ when $\boldsymbol{x}$ is constrained to lie inside or on the surface of the *confidence ellipsoid*

$$\{\boldsymbol{x} | (\boldsymbol{b} - \boldsymbol{A}\boldsymbol{x})^T(\boldsymbol{b} - \boldsymbol{A}\boldsymbol{x}) \le r_0 + \kappa^2\}. \tag{29}$$

But since the regression model (18) is underdetermined, that ellipsoid is open-ended in most directions and the intervals obtained for most $\boldsymbol{w}$ vectors would be $[\hat{\phi}_{lo}, \hat{\phi}^{up}] = [-\infty, +\infty]$. To get nontrivial confidence bounds, it is necessary to impose the constraints (21), defining

$$\tilde{\phi}_{lo} = \min_{\boldsymbol{x}}\{\boldsymbol{w}^T\boldsymbol{x} | (\boldsymbol{b} - \boldsymbol{A}\boldsymbol{x})^T(\boldsymbol{b} - \boldsymbol{A}\boldsymbol{x}) \le r_0 + \kappa^2, \boldsymbol{p} \le \boldsymbol{x} \le \boldsymbol{q}\}, \tag{30}$$

$$\tilde{\phi}^{up} = \max_{\boldsymbol{x}}\{\boldsymbol{w}^T\boldsymbol{x} | (\boldsymbol{b} - \boldsymbol{A}\boldsymbol{x})^T(\boldsymbol{b} - \boldsymbol{A}\boldsymbol{x}) \le r_0 + \kappa^2, \boldsymbol{p} \le \boldsymbol{x} \le \boldsymbol{q}\}. \tag{31}$$

These are very difficult numerical problems which the *FERDIT* algorithm avoids by extending the classical analysis to the regularized model (22) to get suboptimal approximations to the above bounds. More precisely, it works by successively choosing the vectors $\boldsymbol{w}_i$ to be the columns $\boldsymbol{e}_i$ of the matrix $\boldsymbol{I}_{153}$ and computing, for each separate $x_i = \boldsymbol{w}_i^T\boldsymbol{x}$, the value λ which produces the smallest approximate confidence interval. This is done by noting that every λ in the interval $[0, \infty)$ corresponds to a distinct, unique convex combination of the confidence ellipsoid (29) and the circumscribing ellipsoid for the *a priori* constraint region in (21). Each such convex combination contains the intersection of the two parent ellipsoids, so it is also an α-level confidence ellipsoid for the estimate, and hence can be used to compute α-level confidence intervals by the usual classical method. The *FERDIT* method seeks, for each separate window vector $\boldsymbol{w}_i = \boldsymbol{e}_i$, the value of λ which gives the tightest possible confidence interval for $x_i = \boldsymbol{w}_i^T\boldsymbol{x}$. It is not possible to write closed form expressions for the optimal λs, but their values can be easily and stably computed by the secant method. The results obtained from applying these procedures to the present problem are plotted as the

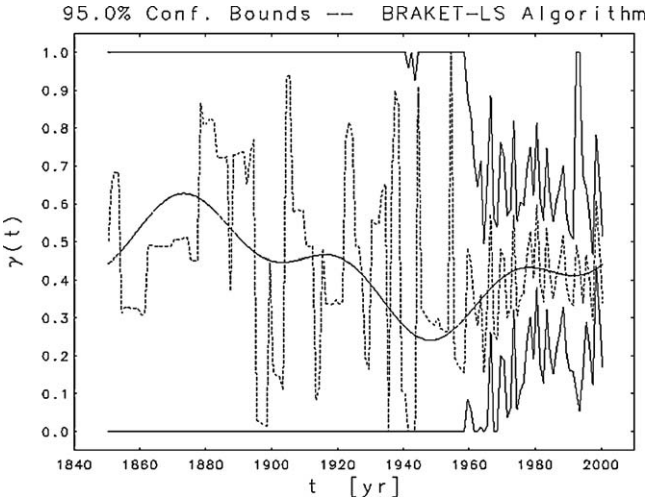

Fig. 7. Inverse problem estimates for the vector $\boldsymbol{\gamma}$. The lowest and highest solid curves are the *BRAKET-LS* 95% confidence bounds ($\kappa = 1.960$), and the dashed curve is the FERDIT estimate (25). The smooth solid curve is the $n_h = 3$ harmonic approximation estimate for $\gamma(t)$, i.e., the magenta curve in Fig. 5.

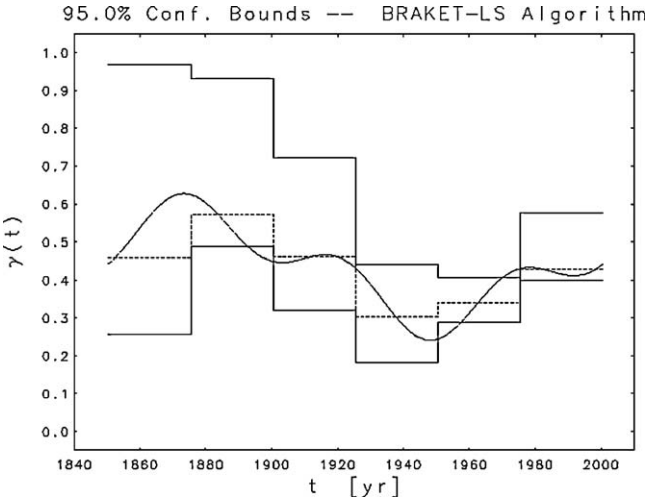

Fig. 8. *BRAKET-LS* bounds and *FERDIT* estimates for 6 nonoverlapping 25-year averages of $\gamma(t)$. The upper and lower piecewise constant curves are the 95% confidence bounds ($\kappa = 1.960$), and the dashed piecewise constant curve is the estimate. The smooth curve is the $n_h = 3$ forward problem estimate for $\gamma(t)$.

dashed curve in Fig. 7, where the indicated upper and lower bounds are not the *FERDIT* approximations, but rather are the optimal bounds computed directly from Eqs. (30) and (31) using O'Leary's BRAKET-LS algorithm [12]. Note that the O'Leary algorithm was not able to really improve on the initial *a priori* bounds until the beginning, in 1958, of the yearly atmospheric measurements at the South Pole. Before that, the uncertainties in the concentration data were about 4 times larger and there were measured data for only 40 of the 108 years.

Better results can be gotten from the less ambitious problems obtained by using vectors $\boldsymbol{w}_k$ designed to give estimates of the average values of $\gamma(t)$ over time subintervals of the total record. The results for 6 nonoverlapping 25-year subintervals are shown in Fig. 8. The pre-1925 uncertainties are large, but the bounds and the *FERDIT* estimates give good agreement with the $\gamma(t)$ estimated from the $n_h = 3$ harmonic expansion approximation.

5. Summary and conclusions

The results in Fig. 8 indicate that the estimates in (12) provide a $\hat{\gamma}(t)$ that reliably establishes a direct connection between man-made CO_2 emissions (from fossil fuel use and land use changes) and global warming. That connection

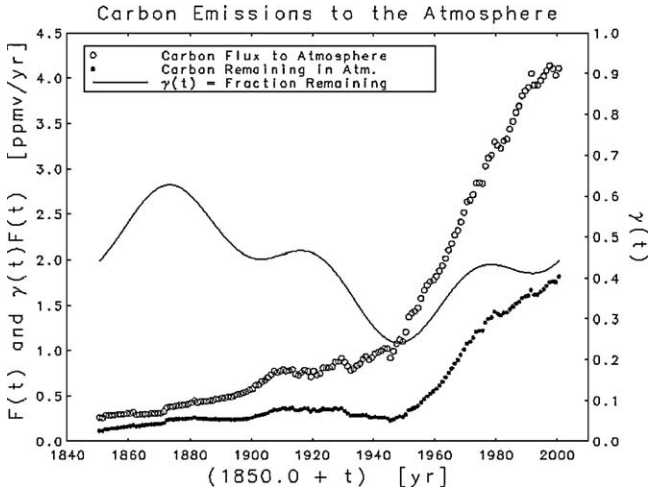

Fig. 9. Man-made CO_2 emissions. The uppermost curve is a plot of the total emission measurements $F(t_i)$. The smooth curve in the middle is the $\hat{\gamma}(t)$ generated by the estimates (12). It is the same as the magenta curve in Fig. 5. The lower curve is a plot of the products $\gamma(t_i)F(t_i)$, the estimated emissions remaining in the atmosphere.

is illustrated in Figs. 9 and 10. The lower curve in Fig. 9 is a plot of the products $\gamma(t_i)F(t_i)$ which were integrated to obtain the dashed curve in the upper plot of Fig. 10. That curve was substituted into Eq. (3) to get the model for the temperature anomaly fit shown as a solid curve in the lower plot. Thus the temperature model was effectively

$$T(t) = T_0 + \eta \left[\hat{c}_{1850} + \hat{A}_0 \int_0^t F(\tau)\,\mathrm{d}\tau + \sum_{k=1}^{3} \hat{A}_k \int_0^t \cos(\omega_k \tau) F(\tau)\,\mathrm{d}\tau \right.$$
$$\left. + \sum_{k=1}^{3} \hat{B}_k \int_0^t \sin(\omega_k \tau) F(\tau)\,\mathrm{d}\tau + \hat{\delta} S(t) - 277.04 \right] + A \sin\left[\frac{2\pi}{\tau}(t + \phi) \right],$$

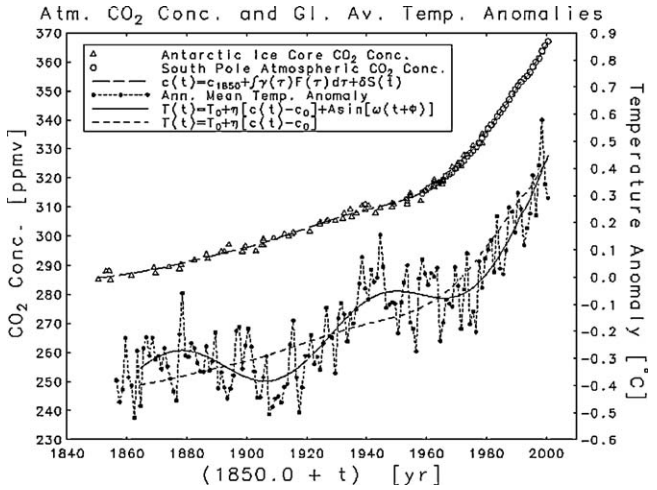

Fig. 10. The connection between CO_2 emissions and global warming. The dashed curve in the upper plot was generated by Eq. (11) using the estimates in (12). It is the same as the magenta curve in Fig. 4. The concentration measurements in the upper plot were used only to determine the estimates (12). The solid curve in the lower plot is the fit of the model (3) to the temperature anomaly measurements using the dashed curve in the upper plot for $c(t)$. The dashed curve in the lower plot is the baseline part of the temperature fit.

with $\hat{c}_{1850}$, $\hat{A}_0$, the $\hat{A}_k$ and $\hat{B}_k$, and $\hat{\delta}$ given by (12). Fitting this model, with $t = 0$ at epoch 1850.0, to the measured $T(t_i)$ gave estimates

$$\begin{aligned}
\hat{T}_0 &= (-0.511 \pm .017)\,(^\circ\mathrm{C}),\\
\hat{\eta} &= (0.01055 \pm .00046)\,(^\circ\mathrm{C/ppmv}),\\
\hat{A} &= (0.100 \pm .012)\,(^\circ\mathrm{C}),\\
\hat{\tau} &= (71.2 \pm 2.2)\,(\mathrm{yr}),\\
\hat{\phi} &= (-7.1 \pm 2.6)\,(\mathrm{yr}),
\end{aligned} \tag{32}$$

which are not very different from those in Eq. (4). And the fit itself is very similar to the one in Fig. 2. The main difference is that here, man-made emissions are indicated as the cause of the warming.

Finally, the $\gamma(t)$ estimates shown in Fig. 8 appear to exhibit a slight overall downward trend. This impression is reinforced by the confidence interval bounds, even though the intervals are quite broad in the first half of the record. If the effect is real, it might be a mixed blessing. Retaining a smaller fraction of the ever increasing emissions might slow down the global warming, but the CO_2 not retained in the atmosphere must go somewhere else. If it goes into the oceans, it could further exacerbate the problems of growing oceanic acidity.

Acknowledgements

The author would like to thank Drs. Dianne P. O'Leary and Anastase Nakassis for helpful advice and criticisms of the manuscript and two anonymous referees for suggestions for improving it.

References

[1] Y. Bard, Nonlinear Parameter Estimation, Academic Press, New York, 1974, Chapter 7.
[2] Carbon Dioxide Information Analysis Center, Oak Ridge National Laboratory, Oak Ridge, TN, 2010. http://cdiac.ornl.gov/faq.html.
[3] W.C. Clark, Carbon Dioxide Review 1982, Oxford University Press, New York, 1982.
[4] D.M. Etheridge, L.P. Steele, R.L. Langerfelds, R.J. Francey, J.M. Barnola, V.I. Morgan, Historical CO_2 Records from the Law Dome DE08, DE08-2, and DSS Ice Cores, Trends: A Compendium of Data on Global Change, CDIAC, Oak Ridge, TN, 1998, http://cdiac.ornl.gov/trends/co2/lawdome.html.
[5] F.A. Graybill, Theory and Application of the Linear Model, Duxbury Press, North Scituate, MA, 1976.
[6] L. Gu, D.D. Baldocchi, S.C. Wofsy, J.W. Munger, J.J. Michalsky, S.P. Urbanski, T.A. Boden, Response of a deciduous forest to the Mount Pinatubo eruption: enhanced photosynthesis, Science 299 (2003) 2035–2038.
[7] R.A. Houghton, Carbon flux to the atmosphere from land-use changes: 1850–2005, Trends: A Compendium of Data on Global Change, CDIAC, Oak Ridge, TN, 2008, http://cdiac.ornl.gov/trends/landuse/houghton/houghton.html.
[8] P.D. Jones, M. New, D.E. Parker, S. Martin, I.G. Rigor, Surface air temperature and its variations over the last 150 years, Rev. Geophys. 37 (1999) 173–199, http://www.cru.uea.ac.uk/cru/data/temperature/.
[9] C.D. Keeling, T.P. Whorf, Atmospheric CO_2 concentrations derived from flask air samples at sites in the SIO network, Trends: A Compendium of Data on Global Change, CDIAC, Oak Ridge, TN, 2004, http://cdiac.ornl.gov/trends/co2/sio-keel-flask/sio-keel-flaskspo.html.
[10] G. Marland, T.A. Boden, R.J. Andres, Global, regional and national CO_2 emissions, Trends: A Compendium of Data on Global Change, CDIAC, Oak Ridge, TN, 2008, http://cdiac.ornl.gov/trends/emis/tre_glob.html.
[11] A. Neftel, H. Friedli, E. Moor, H. Lötscher, H. Oeschger, U. Singenthaler, B. Stauffer, Historical CO_2 record from the Siple Station ice core, Trends: A Compendium of Data on Global Change, CDIAC, Oak Ridge, TN, 1994, http://cdiac.ornl.gov/trends/co2/siple.html.
[12] D.P. O'Leary, B.W. Rust, Confidence intervals for inequality-constrained least squares problems, with applications to ill-posed problems, SIAM J. Sci. Stat. Comput. 7 (1986) 473–489.
[13] J.E. Pierce, B.W. Rust, Constrained least squares interval estimation, SIAM J. Sci. Stat. Comput. 6 (1985) 670–683.
[14] B.W. Rust, B.J. Thijsse, Data-based models for global temperature variations, in: H.R. Arabnia, J.Y. Yang, M.Q. Yang (Eds.), Proceedings of the 2007 International Conference on Scientific Computing, CSREA Press, Las Vegas, NV, 2007, pp. 10–16.
[15] M.E. Schlesinger, N. Ramankutty, An oscillation in the global climate system of period 65–70 years, Nature 367 (1994) 723–726.
[16] B.J. Thijsse, B.W. Rust, Freestyle data fitting and global temperatures, Comput. Sci. Eng. 10 (2008) 49–59.